International Journal of Microwave and Wireless Technologies

cambridge.org/mrf

Analytical modeling of antisymmetric split-ring resonators coupled with transmission line

Vojislav Milosevic[1], Radovan Bojanic[2] and Branka Jokanovic[1]

[1]Institute of Physics, University of Belgrade, Pregrevica 118, 11080 Belgrade, Serbia and [2]Technische Universiteit Eindhoven, P.O. Box 513, 5600 MB Eindhoven

Research Paper

Cite this article: Milosevic V, Bojanic R, Jokanovic B (2019). Analytical modeling of antisymmetric split-ring resonators coupled with transmission line. *International Journal of Microwave and Wireless Technologies* **11**, 359–367. https://doi.org/10.1017/S1759078719000308

Received: 31 October 2018
Revised: 20 February 2019
Accepted: 21 February 2019
First published online: 25 March 2019

Key words:
coupled-mode theory; equivalent circuit; S-parameters; split-ring resonator; coupled oscillators

Author for correspondence:
Vojislav Milosevic,
E-mail: vojislav.milosevic@ipb.ac.rs

Abstract

Coupled-mode theory is applied to obtain an analytic form of scattering parameters for a class of transmission line metamaterials with antisymmetric split-rings. The same structure is modeled with equivalent circuit, which includes electric and magnetic coupling with the line and inter-resonator coupling. Modified even/odd analysis is used to obtain scattering parameters from the equivalent circuit. These two methods are shown to be equivalent in a narrow band, and their constants related. The obtained results are compared with full-wave simulations and measurements, and it is shown that both methods give accurate approximation in one octave frequency band. The derived analytic expressions are suitable for study of resonant phenomena, with potential practical applications for filters, phase shifters, delay lines, and sensors.

Introduction

Since the metamaterials were introduced [1], they served as an inspiration for novel ideas in different fields, not always strictly related to the original concept. Notably, transmission lines (TLs) loaded with sub-wavelength resonators, also known as metamaterial TLs (MMTLs) or composite right-/left-handed (CRLH) TLs, have been extensively studied in the context of applications in microwave engineering [2, 3]. Loading elements can be either lumped, or in the form of electrically small resonators, such as the split-ring resonators (SRRs). The latter has been used for development of various microwave circuits, such as miniaturized filters [4], displacement sensors [5], phase shifters [6], for common mode suppression in differential lines [7], improved antennas [8], etc. It should be noted that the position and orientation of the gap in SRR with respect to the TL has a great impact on overall characteristics of the loaded TL [9, 10], which can be used for design of reconfigurable devices and antennas.

Although electromagnetic problems involving MMTLs are usually solvable numerically, it is still desirable to have some simplified model, which can facilitate optimization tasks, as well as provide insight into underlying physics of more complex phenomena. To this end, equivalent electric circuits, composed of lumped elements, are typically used. A considerable amount of work was done on this topic, and it was shown how equivalent circuits can be used to model microstrip and CPW lines coupled with SRRs and complementary SRRs, with or without vias [11, 12]. Arbitrary position of SRR gaps with respect to TL can lead to cross-polarization effect, and it can be included as mixed coupling [10, 13]. It was shown that the bandwidth of the equivalent circuit validity can be greatly increased, without increasing the number of unknowns, by using two Π-cells, instead of one, to model the TL [13].

Many interesting phenomena in metamaterials are manifested by characteristic spectral line shapes of scattering parameters. These include Fano resonance and classical analogue of electromagnetically-induced transparency (EIT) which is characterized by narrow transmission peak within a wider stopband and strong dispersion accompanied by high group delay values [14–16]. For the study of such systems, it is highly desirable to have approximate analytic forms of scattering parameters in the vicinity of resonances. While in principle derivable from the equivalent circuit, this may be a difficult task, in part because the approximation can introduce unphysical resonances. As an alternative, coupled-mode theory (CMT) can be used [17, 18]. In this paper, both CMT and equivalent-circuit analysis will be applied to derive analytic form of scattering parameters for a class of MMTL unit cells with antisymmetric SRRs. Both approaches will be compared and their equivalence will be investigated.

Microstrip TL loaded with SRRs with various gap positions, are shown in Figs 1 and 2. In general, two SRRs will have some coupling between them, so two resonances may be expected due to mode splitting. The geometries in Fig. 1 have mirror symmetry with respect to the plane which is perpendicular to the substrate along the middle of the TL. Due to this symmetry, one of the resonances cannot be excited, which is why they will exhibit single resonance in their transmission spectrum [13]. On the other hand, geometries in Fig. 2, which are named *antisymmetric*, do not possess a mirror symmetry plane, instead they are symmetric

CAMBRIDGE UNIVERSITY PRESS

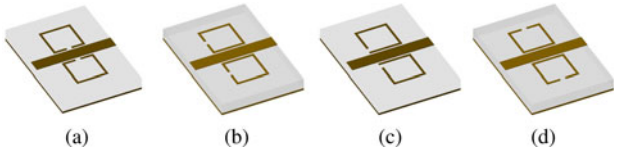

Fig. 1. Symmetric configuration of two SRRs coupled with microstrip line.

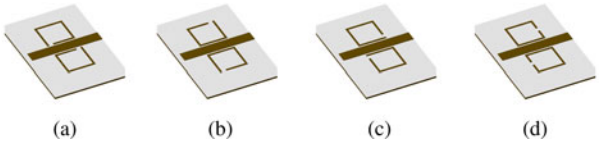

Fig. 2. Antisymmetric configuration of two SRRs coupled with microstrip line.

for the 180° rotation around the central point. Antisymmetry can be exploited in filter design to introduce additional transmission zeros [19]. Unlike structures with mirror symmetry, they have two resonances in transmission spectrum, which can be tuned independently. This adds additional degree of freedom to engineer dispersion in antisymmetric structures, which is of great importance for many practical applications, like high-order filters, phase shifters and delay lines. Proper coupling between the two resonant modes can lead to classical analogue of EIT, with extremely narrow resonant peaks, which is suitable for sensing applications [20].

This paper is organized as follows: in the section "Coupled-mode theory" we lay out the CMT for the case of the TL coupled with two resonators, and then apply the antisymmetry of the system and derive scattering parameters; in the section "Equivalent circuit approach" we propose the equivalent circuit for the structure, and show how even/odd analysis can be used to simplify the analysis, and again derive scattering parameters in a form which is comparable to the CMT. Finally, in the section "Results and comparison" we compare the approximation of *S*-parameters obtained by both methods with the results of full-wave simulations and measurements.

Analysis

Coupled-mode theory

The CMT is based on a representation of a coupled system using the modes of an uncoupled system, which can be rigorously derived by using the orthogonal mode expansion or variational principle [17]. When the coupling is relatively weak and individual modes are clearly distinguishable, as is the case in systems under consideration, only a few modes need to be taken into account to obtain good approximation, and the results are easily understood intuitively. Historically, the CMT was first applied in microwave engineering for the analysis of tubes, oscillators and waveguides back in 1950s. However later it became more associated with optical resonators in photonics [17, 18].

The independent variable in CMT can be either the spatial coordinate or time; depending on which we speak about mode coupling in space or time [21]. The spatial type of CMT has been used for the analysis of periodic structures, e.g. the microstrip line with periodic perturbations in the ground plane or conductor strip, also known as photonic band-gap (PBG) structures [22]. Temporal CMT has been used to analyze classical analogue of EIT [23]. However, to the authors' best knowledge, this is the first time it has been applied to microwave MMTLs.

General schematic representation of the TL coupled with two resonators, corresponding to the geometries shown in Figs 1 and 2 is given in Fig. 3 (at this point no specific symmetry of this system is assumed, and resonant frequencies and couplings with the line can be different). In CMT, the resonators are first considered to be not coupled to the TL (but can be coupled between themselves). To describe the excitation the of resonators, so-called positive frequency amplitudes, $\alpha_{1,2}$, are used. Their magnitude equals the square root of the power stored in a mode, and the argument corresponds to the phase of oscillations [21]. The relationship between α_i coefficients and voltage and current of the resonator is analogous to the relationship between incident and reflected power waves, *a*, *b*, used for definition of *S*-parameters, and voltage and current on the TL. Because of this, CMT description relates more directly with *S*-parameters than the equivalent circuit, as it will be shown later.

In the following, the matrix approach from Ref. [24] will be used (with slightly adjusted notation to conform to microwave engineering conventions), so the reader is referred there for rigorous proofs of the used relations. Assuming no ohmic losses, time dependence of the resonant modes will be described with two coupled differential equations:

$$\frac{\partial}{\partial t}\begin{bmatrix}\alpha_1\\ \alpha_2\end{bmatrix} = j\mathbf{\Omega}\begin{bmatrix}\alpha_1\\ \alpha_2\end{bmatrix}, \quad \mathbf{\Omega} = \begin{bmatrix}\omega_1 & \kappa\\ \kappa^* & \omega_2\end{bmatrix}, \tag{1}$$

where $\omega_{1,2}$ are resonant frequencies, κ is the mutual coupling coefficient, and * superscript indicates complex conjugate.

The TL is described by incident and reflected waves (as per usual definition of *S*-parameters), which are related by non-resonant 'direct' scattering matrix $\mathbf{S}^{(0)}$ (corresponding to the isolated TL):

$$\begin{bmatrix}b_1\\ b_2\end{bmatrix} = \mathbf{S}^{(0)}\begin{bmatrix}a_1\\ a_2\end{bmatrix}. \tag{2}$$

When coupling between the resonators and TL is introduced, two effects occur:(1) incident waves can excite the resonant modes; (2) power from resonant modes leaks in the TL. In other words, the TL appears both as a drive and as a decay channel for the resonators. Mathematically, the coupling is treated as a first-order perturbation, which is included in equations (1) and (2) by linear terms, proportional to the coefficients of the matrix $\mathbf{D} = [d_{ij}]$, where indices in the subscript represent row and column of matrix element (see Fig. 3):

$$\frac{\partial}{\partial t}\begin{bmatrix}\alpha_1\\ \alpha_2\end{bmatrix} = (j\mathbf{\Omega} - \mathbf{\Gamma})\begin{bmatrix}\alpha_1\\ \alpha_2\end{bmatrix} + \mathbf{D}^T\begin{bmatrix}a_1\\ a_2\end{bmatrix}, \tag{3}$$

$$\begin{bmatrix}b_1\\ b_2\end{bmatrix} = \mathbf{S}^{(0)}\begin{bmatrix}a_1\\ a_2\end{bmatrix} + \mathbf{D}\begin{bmatrix}\alpha_1\\ \alpha_2\end{bmatrix}, \tag{4}$$

where $\mathbf{\Gamma} = (1/2)\mathbf{D}^\dagger\mathbf{D}$ is the matrix of damping terms due to power leakage from the resonators into the TL [17, 18, 21]. In the preceding expressions, *T* superscript indicates matrix transpose, and dagger (†) stands for Hermitian transpose.

By taking into account the rotational symmetry of the structures in Fig. 2, i.e. by requiring that the system is unchanged upon 180° rotation, we can deduce the form of the **D**, **S**, and **Ω**

https://doi.org/10.1017/S1759078719000308 Published online by Cambridge University Press

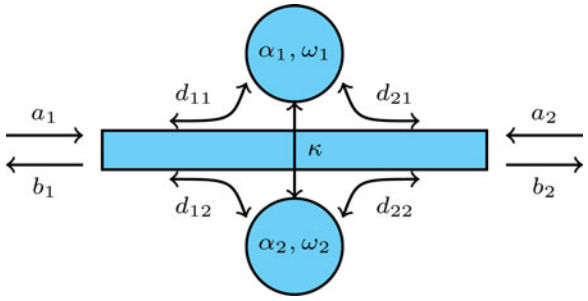

Fig. 3. TL coupled with two resonant modes.

matrices:

$$\mathbf{S}^{(0)} = \begin{bmatrix} S_{11}^{(0)} & S_{21}^{(0)} \\ S_{21}^{(0)} & S_{11}^{(0)} \end{bmatrix}, \quad \mathbf{D} = \begin{bmatrix} d_1 & d_2 \\ d_2 & d_1 \end{bmatrix}, \quad \Omega = \begin{bmatrix} \omega_0 & -\kappa \\ -\kappa & \omega_0 \end{bmatrix}, \tag{5}$$

where $\kappa \in R$ in this case. Under steady-state excitation and after substituting (3) and (5) into (4), the resulting transmission through the system is straightforwardly obtained:

$$S_{21} = S_{21}^{(0)} + \frac{(d_1 + d_2)^2}{2j(\omega - \omega_0 - \kappa) + |d_1 + d_2|^2} - \frac{(d_1 - d_2)^2}{2j(\omega - \omega_0 + \kappa) + |d_1 - d_2|^2}, \tag{6}$$

and reflection:

$$S_{11} = S_{11}^{(0)} + \frac{(d_1 + d_2)^2}{2j(\omega - \omega_0 - \kappa) + |d_1 + d_2|^2} + \frac{(d_1 - d_2)^2}{2j(\omega - \omega_0 + \kappa) + |d_1 - d_2|^2}. \tag{7}$$

In the expressions (6) and (7), the first fraction corresponds to the even mode and second to the odd mode, while resonant frequencies are $\omega_\pm = \omega_0 \pm \kappa$ and Q-factors:

$$Q_\pm = \omega_\pm / \gamma_\pm, \quad \gamma_\pm = |d_1 \pm d_2|^2 \tag{8}$$

where (+) sign corresponds to the even mode, and (−) to the odd mode.

Additionally, it can be shown that the following relation holds:

$$\mathbf{S}^{(0)}\mathbf{D}^* = -\mathbf{D}, \tag{9}$$

which enables determining the phase of elements of matrix $\mathbf{D}$ [24].

To determine the values of constants in the preceding expressions for particular geometry, several approaches can be used, such as curve-fitting to the results of measurements or simulations, or derivation from the parameters of the equivalent circuit, as it will be shown later. However, it should be stressed that CMT is an independent method, and the constants can also be directly obtained from field patterns of resonant modes, as it was demonstrated in [17].

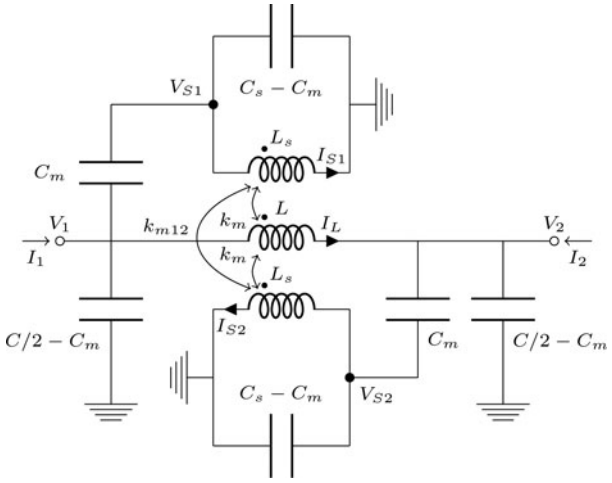

Fig. 4. Equivalent circuit of the asymmetrically coupled split-ring resonators in Fig. 2.

Equivalent circuit approach

The proposed equivalent circuit for the antisymmetric configurations (Fig. 2) is shown in Fig. 4. In addition to the most commonly used model, where only magnetic coupling is present [11, 13], here both the electric and magnetic coupling with the line and mutual coupling between SRRs is included. The proposed circuit model is electrically symmetric, hence it is desirable to analyze it with even/odd-mode excitation. However, there is no mirror symmetry, so the even- and odd-mode admittances cannot be obtained in a standard way, by placing the electric and magnetic wall in the symmetry plane. Instead, it will be shown how rotational symmetry of the structure can be exploited to obtain the even/odd-mode admittance.

We start by observing that all circuit responses are bilinear functions of input parameters, e.g.

$$I_{S1} = \mathcal{L}_{I_{S1}}(V_1, V_2) = -\mathcal{L}_{I_{S1}}(-V_1, -V_2). \tag{10}$$

Due to the antisymmetry, the following has to hold (for the reference directions given in Fig. 4):

$$I_{S2} = \mathcal{L}_{I_{S2}}(V_1, V_2) = \mathcal{L}_{I_{S1}}(V_2, V_1). \tag{11}$$

Using (10) and (11), the relations for circuit responses under even and odd excitation can be derived, and they are summarized in Table 1. Based on that, we can obtain a simplified circuits for the even and odd excitation, which are shown in Fig. 5. We can now calculate the even- and odd-mode admittance, $y_{e,o}$, normalized on $Y_0 = \sqrt{C/L}$

$$\begin{aligned} y_e &= y_e^\Pi + \frac{j}{2}\frac{\omega}{\omega_{LC}}\frac{2\gamma_e^2}{1 - \omega^2/\omega_e^2}, \\ y_e^\Pi &= \frac{j}{2}\frac{\omega}{\omega_{LC}}\left(1 - 2k_e^2\right), \\ y_o &= y_o^\Pi + \frac{j}{2}\frac{\omega}{\omega_{LC}}\frac{2\gamma_o^2}{1 - \omega^2/\omega_o^2}, \\ y_o^\Pi &= \frac{j}{2}\frac{\omega}{\omega_{LC}}\left(1 - 2k_e^2\right) - 2j\frac{\omega_{LC}}{\omega}, \end{aligned} \tag{12}$$

https://doi.org/10.1017/S1759078719000308 Published online by Cambridge University Press

Table 1. Equivalent circuit responses under the even and odd excitation

Even	Odd
$V_1 = V_2$	$V_1 = -V_2$
$I_{S1} = I_{S2}$	$I_{S1} = -I_{S2}$
$V_{S1} = V_{S2}$	$V_{S1} = -V_{S2}$
$I_L = 0$	I_L arbitrary.

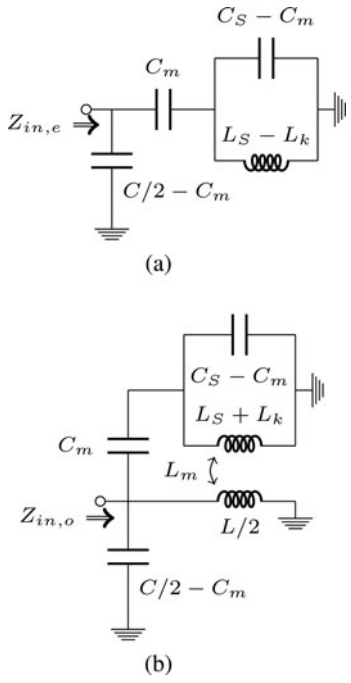

Fig. 5. Equivalent circuits for (a) even; (b) odd-mode excitation (where $L_k = k_{m12}L_S$ is the mutual inductance between the rings).

where

$$\begin{aligned}\gamma_e &= k_e,\\ \gamma_o &= 2\omega_{LC}\sqrt{L_S C_S}k_m - k_e,\\ \omega_e &= 1/\sqrt{L_S C_S(1-k_{m12})},\\ \omega_o &= 1/\sqrt{L_S C_S(1+k_{m12}-2k_m^2)},\\ \omega_{LC} &= 1/\sqrt{LC},\end{aligned} \tag{13}$$

and k_e, electric coupling coefficient, is defined as:

$$k_e = C_m/\sqrt{CC_S}. \tag{14}$$

In (12), we separated the non-resonant parts of the admittances under the terms $y_{e,o}^{\Pi}$. They represent the even/odd-mode admittance of the Π-cell in Fig 4, i.e. of the TL only[1]. This notation will allow us to compare the results from the coupled mode theory with an equivalent circuit approach much easier, as it will become clear later on. The transmission coefficient, S_{21}, is [25]:

$$S_{21} = \frac{1}{2}(S_{11,e} - S_{11,o}) = \frac{1}{2}\left(\frac{1-y_e}{1+y_e} - \frac{1-y_o}{1+y_o}\right). \tag{15}$$

The non-resonant part of the transmission can be calculated using the term $y_{e,o}^{\Pi}$ (12):

$$S_{21}^{\Pi} = \frac{1}{2}(S_{11e}^{\Pi} - S_{11o}^{\Pi}), \quad S_{11e,o}^{\Pi} = \frac{1-y_{e,o}^{\Pi}}{1+y_{e,o}^{\Pi}}, \tag{16}$$

which is equivalent to the "direct" scattering matrix $\mathbf{S}^{(0)}$ from the section "Coupled-mode theory". By substituting (12), (13), and (16), after straight forward but tedious calculations, the final expression for the transmission is obtained:

$$S_{21} = S_{21}^{\Pi} - \frac{S_{11,e}^{\Pi}\gamma'_e}{j(\omega^2 - \varpi_e^2) + \gamma'_e} + \frac{S_{11,o}^{\Pi}\gamma'_o}{j(\omega^2 - \varpi_o^2) + \gamma'_o}, \tag{17}$$

where

$$\gamma'_{e,o} = \mathrm{Re}\left\{\frac{1}{1+y_{e,o}^{\Pi}}\right\}\frac{\omega}{\omega_{LC}}\omega_{e,o}^2\gamma_{e,o}^2, \tag{18}$$

$$\varpi_{e,o} = \omega_{e,o} - \mathrm{Im}\left\{\frac{1}{1+y_{e,o}^{\Pi}}\right\}\frac{\omega}{\omega_{LC}}\omega_{e,o}^2\gamma_{e,o}^2. \tag{19}$$

The form of (17) was deliberately chosen to stress the equivalence with the result of the coupled mode approach [cf. (6)]. However, the important difference is that, instead of the constant values in (6), we have the functions of frequency in (17), defined by (18) and (19). Nevertheless, they are slowly changing with frequency compared to the resonant terms, and therefore the two approaches are equivalent in a narrow frequency band around the resonances. In Table 2, it is shown how the circuit parameters can be used to calculate the coupled-mode constants, by fixing ω at the desired frequency of interest.

Frequency dependence of modes' effective resonant frequencies $\varpi_{e,o}$ and coupling strengths $\gamma_{e,0}'$ in (17)–(19) can be explained as follows. In the equivalent circuit model, Π-cell used to represent the TL also acts as a resonator, albeit with a much higher frequency than the SRR modes. Nevertheless, coupling with the line causes frequency-dependent perturbation apparent in (18) and (19). In order to obtain analytic form of transmission or reflection which is simple enough to be intuitively understood, such as (17), one usually wants to neglect such perturbations. However, this may be very difficult task when starting from Kirchhoff's laws for equivalent circuit, because it is not apparent what can and cannot be neglected. In contrast to that, CMT can produce expressions like (6) directly, because it inherently separates transmission medium and resonators, except for the first-order coupling. Therefore, it represents a natural frame for analyzing scattering in systems of coupled resonators.

[1]It should be noted, however, that $y_{e,o}^{\Pi}$ are slightly perturbed compared to the isolated TL, due to the presence of SRRs.

https://doi.org/10.1017/S1759078719000308 Published online by Cambridge University Press

Table 2. Equivalence between the coupled-mode theory constants and equivalent circuit parameters

CMT	Equivalent circuit
ω_+	$\omega_e - \mathrm{Im}\left\{\frac{1}{1+y_e^{\Pi}}\right\}\frac{\omega\omega_e^2}{\omega_{LC}(\omega+\omega_e)}\gamma_e^2$
ω_-	$\omega_o - \mathrm{Im}\left\{\frac{1}{1+y_o^{\Pi}}\right\}\frac{\omega\omega_o^2}{\omega_{LC}(\omega+\omega_o)\gamma_o^2}$
γ_+	$\mathrm{Re}\left\{\frac{1}{1+y_e^{\Pi}}\right\}\frac{2\omega\omega_e^2}{\omega_{LC}(\omega+\omega_e)\gamma_e^2}$
γ_-	$\mathrm{Re}\left\{\frac{1}{1+y_o^{\Pi}}\right\}\frac{2\omega\omega_o^2}{\omega_{LC}(\omega+\omega_o)\gamma_o^2}$

Results and comparison

Validation of equivalence between two methods

In order to validate the presented approaches and compare results, the 3D EM simulation of the structures in Fig. 2 was performed, and they were also fabricated and measured. Relevant dimensions are given in Fig. 6, and dielectric substrate Rogers RO3010, with $\varepsilon_r = 10.2$, is used.

Parameters of the equivalent circuit are determined first. To obtain L, C, and L_S, microstrip line and two nearest SRR arms are modeled as a section of the multi-conductor TL (see Fig. 8). LINPAR software [26] is employed for the numerical evaluation of the quasi-static line parameters. LINPAR provides the per unit length (p.u.l.) inductance and capacitance matrices from which the required parameters L, C, and L_S are obtained, by multiplying with appropriate lengths [13]. Remaining parameters are determined by curve fitting to the results of full-wave simulations.

Nelder-Mead simplex method [27] was used for fitting, with error function integrating the absolute difference (L^1 norm) between simulated data and parametrized model, over spectrum from 4 to 8 GHz:

$$\mathrm{Err} = \int_{f_{\min}}^{f_{\max}} \sum_{i=1}^{2}\sum_{j=1}^{2} \left| S_{ij}^{model} - S_{ij}^{sim} \right| df. \qquad (20)$$

The same procedure was applied in all other instances of curve fitting in this paper.

The coupled-mode constants were obtained using expressions in the right-hand-side of Table 2, which were evaluated for a frequency between resonances. It remains to determine non-resonant direct scattering matrix $\mathbf{S}^{(0)}$, which can be done in several ways. For example, matrix elements could be taken as constants and determined by fitting, or matrix could be obtained from simulation of isolated TL section. Here, $\mathbf{S}^{(0)}$ is calculated from the circuit consisting of the Π-cell only (Fig. 7a), with the same values of L and C as in equivalent circuit. This allows for the best possible comparison between the two models.

The results for two structures in Fig. 2 are shown in Figs 9 and 10, and obtained parameters are summarized in Table 3. It can be observed that the equivalent circuit approach and coupled-mode theory agree almost perfectly around the resonances, while there are discrepancies in the broader band, in accordance with the conclusions from the section "Equivalent circuit approach". Second, both methods show good agreement with EM simulations in both magnitude and phase in case of transmission (S_{21} parameter) in the whole bandwidth; on the other hand, in case of reflection (S_{11} parameter), there is good agreement only in a narrow band around the resonances.

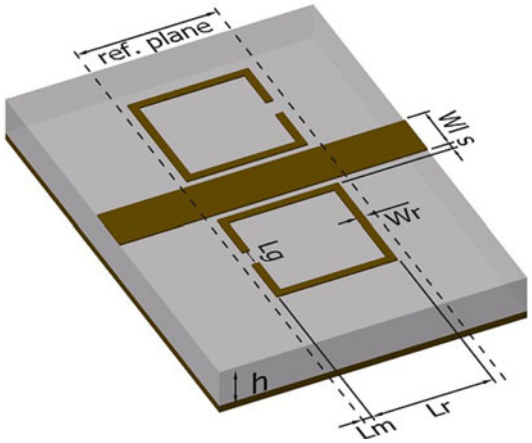

Fig. 6. Relevant dimensions: $h = 1.27$mm, $L_r = 3$ mm, $L_m = 0.25$ mm, $L_g = 0.5$ mm, $W_r = 0.2$ mm, $W_l = 1.2$ mm, and $s = 0.1$ mm.

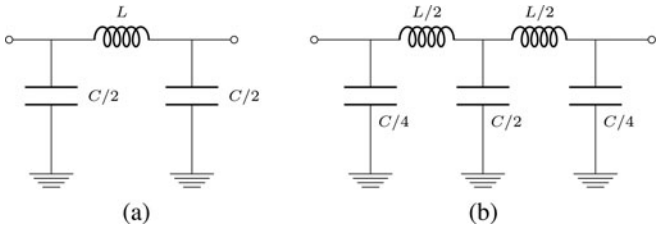

Fig. 7. Equivalent circuit of the TL section only, with (a) one and (b) two Π-cells.

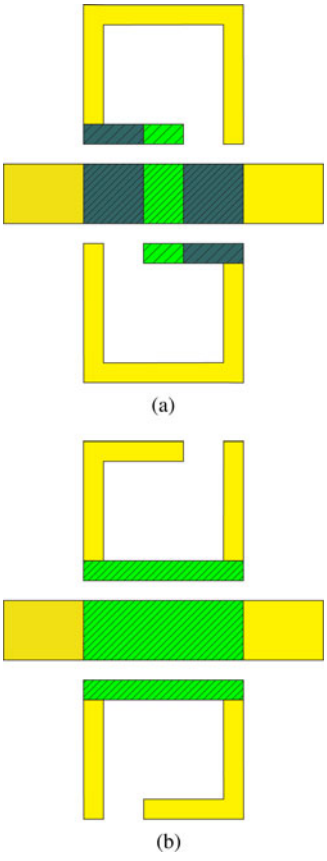

Fig. 8. Determination of circuit parameters based on quasi-static p.u.l. parameters. Coupled line sections are hatched.

https://doi.org/10.1017/S1759078719000308 Published online by Cambridge University Press

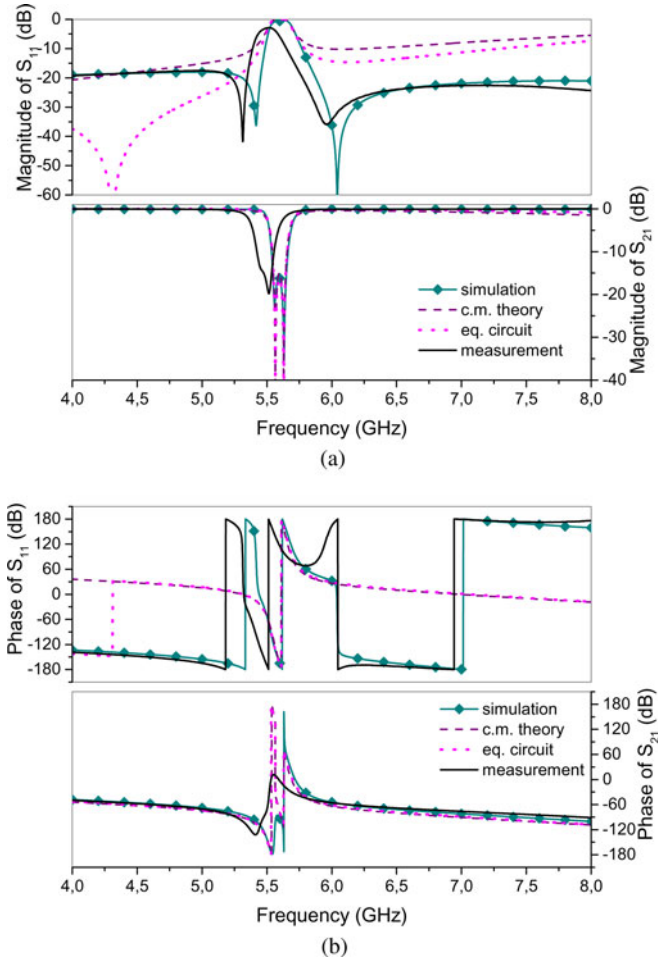

Fig. 9. Magnitude and phase of *S*-parameters for the model in Fig. 2a

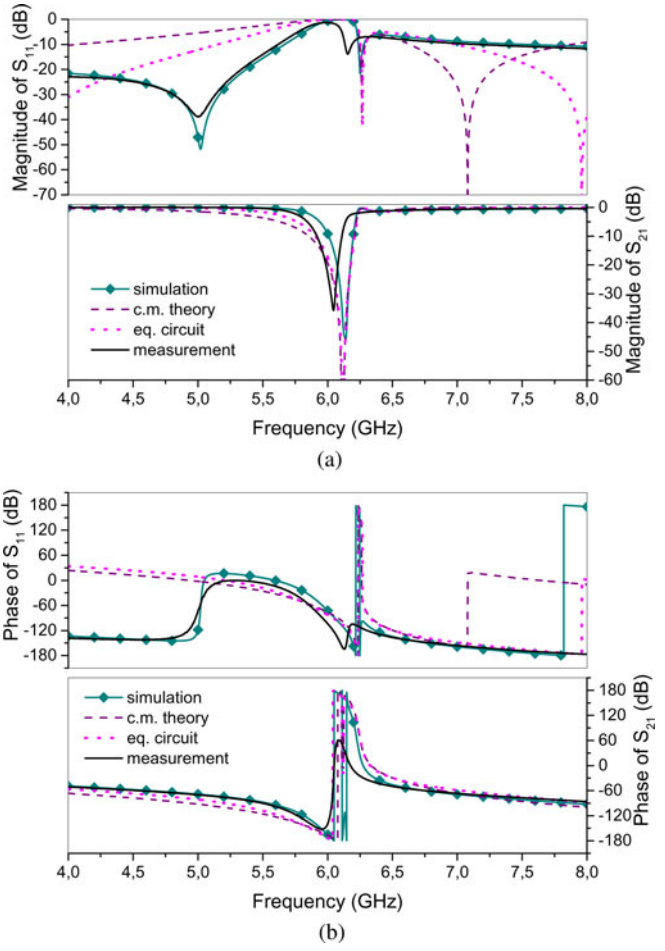

Fig. 10. Magnitude and phase of *S*-parameters for the model in Fig. 2b

Improved results

As the results from the previous section were judged as not completely satisfactory, an effort was made to improve upon them. To this end, equivalent circuit with two Π-cells was used (Fig. 11), since it is expected to give good approximation in a broader bandwidth, compared to simpler circuit in Fig. 4 [13]. It should be noted that both circuits have the same number of unknown parameters, however the topology in Fig. 11 much better reflects the distributed nature of TL. Circuit parameters are determined in the same way as before (L, C, and L_S from the coupled-line section, and the rest by curve-fitting).

In the case of CMT, for the calculation of non-resonant parameters $\mathbf{S}^{(0)}$ TL model with two Π- cells is used (Fig. 7b), to better match the improved equivalent circuit. Then, to obtain the best possible matching, curve fitting procedure is applied for all parameters in the CMT model (L, C of Fig. 7 and $\omega_{\pm}$, $\gamma_{\pm}$). This will generally result in slightly different values of L and C for CMT and equivalent circuit model, which may seem strange at first glance; however, it should be kept in mind that non-resonant part of the equivalent circuit is actually perturbed due to the presence of resonators, as it is noted in the section "Equivalent circuit approach". It is expected that this effect will be more significant in the case of the improved circuit with two Π-cells, because the coupling between SRRs and TL is more distributed. Therefore, independent tuning of L and C is needed in order to account for this perturbation in the CMT model.

Table 3. Results obtained for the models in Fig. 2.

Fig.	2a	2b	Fig.	2a	2b
Equivalent circuit			*Coupled-mode theory*		
L [nH]	1.48	1.47	L [nH]	1.48	1.47
C [pF]	0.8	0.84	C [pF]	0.8	0.84
L_S [nH]	7.97	7.92	ω_+ [GHz]	5.65	6.24
C_S [pF]	0.105	0.09	ω_- [GHz]	5.54	6.13
k_m	0.199	0.35	$\gamma_+[10^8\,\frac{\text{rad}}{\text{s}}]$	3.52	2.21
k_e	0.148	0.109	$\gamma_-[10^8\,\frac{\text{rad}}{\text{s}}]$	3.79	26.5
k_{m12}	0.042	0.08			

New results for all models in Fig. 2 are shown in Fig. 12, and parameters, obtained by the above procedure, are summarized in Table 4. This time, very good agreement has been obtained, not just for S_{21} but also for S_{11}, in the whole bandwidth of one octave. Overall, CMT and equivalent circuit model produce equally good results, the only exception being slight mismatch in the first S_{11} minimum on Fig. 12a. Considering the measurements in Fig. 12, it can be seen that the resonances are wider and shifted to lower frequencies. This is attributed to the presence of losses, which are left out from the EM simulations and analytical studies.

https://doi.org/10.1017/S1759078719000308 Published online by Cambridge University Press

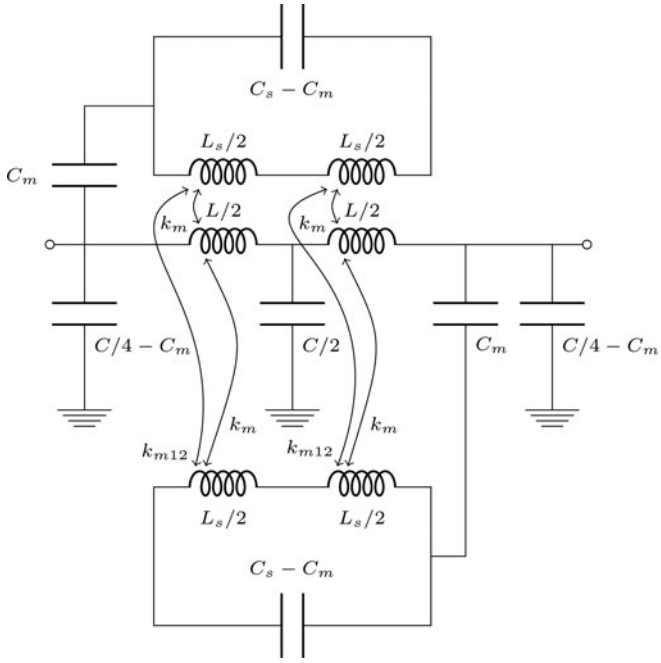

Fig. 11. Equivalent circuit of the antisymmetric structures with two Π-cells.

Table 4. Improved results obtained for the models in Fig. 2.

Fig.	2a	2b	2c	2d
Equivalent circuit				
L [nH]	1.48	1.47	1.47	1.47
C [pF]	0.8	0.84	0.84	0.84
L_S [nH]	7.97	7.91	7.91	7.91
C_S [pF]	0.105	0.09	0.109	0.10
k_m	0.2	0.29	0.276	0.30
k_e	0.15	0.11	0.267	0.24
k_{m12}	0.042	0.07	0.086	0.10
Coupled-mode theory				
ω_+ [GHz]	5.67	6.23	5.81	6.06
ω_- [GHz]	5.52	6.02	5.54	5.76
$\gamma_+[10^8 \frac{\text{rad}}{\text{s}}]$	4.25	2.01	10.8	9.46
$\gamma_-[10^8 \frac{\text{rad}}{\text{s}}]$	3.44	13.8	3.21	5.18
L [nH]	1.46	1.23	1.44	1.39
C [pF]	0.762	0.822	0.734	0.749

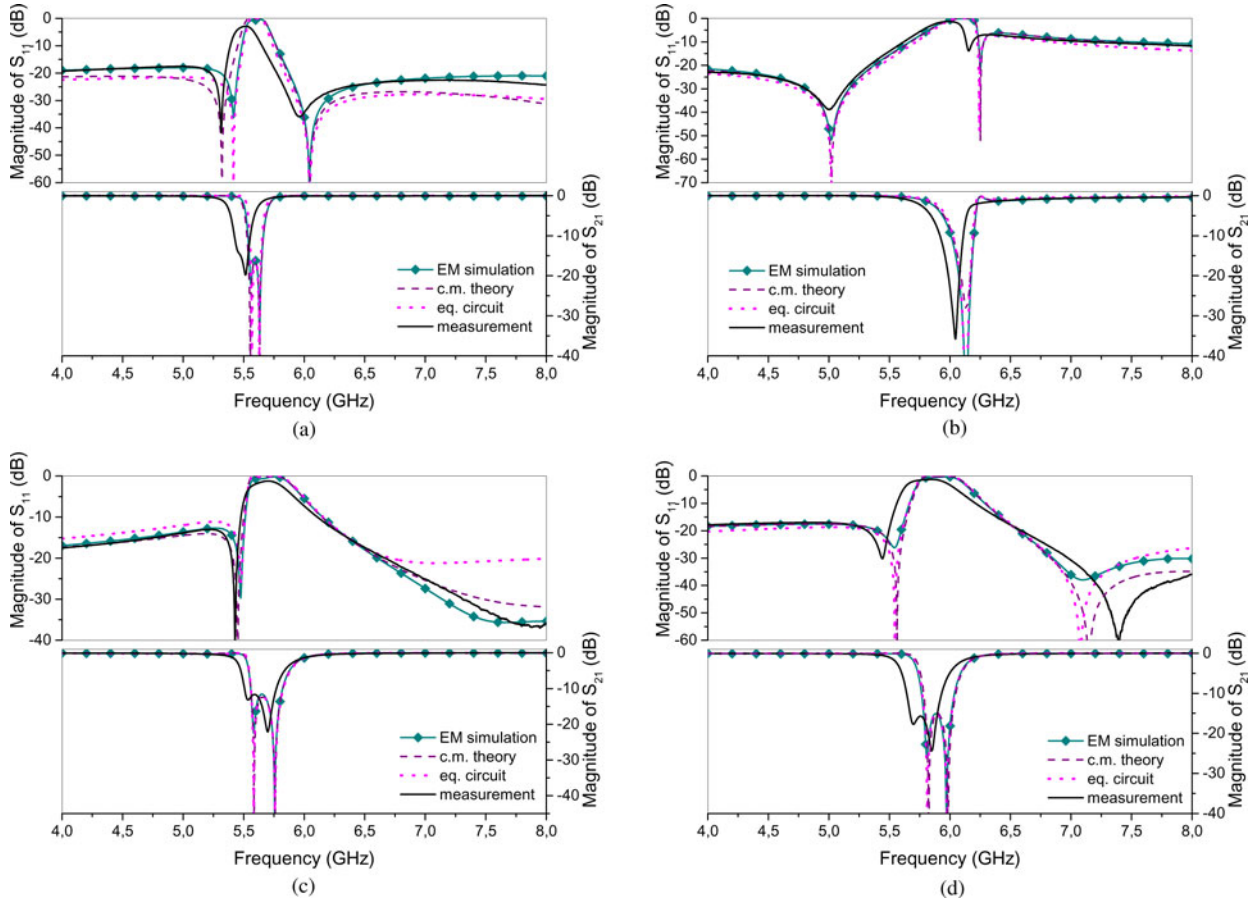

Fig. 12. Comparison of magnitudes of *S*-parameters, obtained by simulation, measurement, equivalent circuit and coupled-mode theory, for the model in Fig. 2a (a), Fig. 2b (b), Fig. 2c (c), and Fig. 2d (d).

https://doi.org/10.1017/S1759078719000308 Published online by Cambridge University Press

It can also be noted that in some cases, such as in Fig. 12b, only a single resonance is visible in the transmission, because the frequency splitting is too small compared to the resonant widths.

By examining the values in Table 4, we can observe that total coupling strength (which may be estimated as $\gamma_+ + \gamma_-$) increases as the SRR gap is moved away from the TL. This can be explained by the current distribution of the SRR, which has the biggest intensity in the arm opposite to the gap. It can also be seen that the fitted values of TL characteristic impedance used in CMT model (Fig. 7b), defined as $Z_C = \sqrt{L/C}$, also varies (last two rows of Table 4). This effect can be explained by the perturbation due to coupling, and it also explains disagreement in the preceding section, since there this perturbation is not accounted for. Consistently, variation in Z_C is largest for the case of strongest coupling (Fig. 2b). Finally, it can also be seen that the coupling causes resonances to shift to higher frequencies.

Conclusion

MMTLs with antisymmetric SRRs possess 180° rotational symmetry around central point and can be analyzed in terms of even and odd excitation. Unlike structures with mirror symmetry, they generally exhibit two resonances in the transmission spectrum that can be tuned independently, making them interesting for various practical applications.

Temporal coupled-mode theory has been applied to analyze the proposed structures. It has been shown how it can easily produce approximate analytic forms of scattering parameters, which makes it a valuable tool for consideration of systems of coupled resonators.

Additionally, equivalent circuit for modeling antisymmetric SRRs coupled with TL is proposed, which includes both the electric and magnetic coupling with the TL and inter-ring coupling. It is shown how the even/odd mode analysis could be used to exploit rotational symmetry of the circuit, allowing simplified calculation of scattering parameters. Both approaches yield the same results in the vicinity of the resonances, while their broadband behavior is generally different. Relations linking parameters in both models are also derived.

Comparison with the *S*-parameters of the simulated and measured structures was made. First results corroborated correlation between two models, since CMT constants were calculated from equivalent circuit parameters and good agreement between them was obtained. However, while there was good agreement with EM simulations in transmission spectra, discrepancies in reflection were more pronounced. Therefore, the improved results are presented; obtained using equivalent circuit with two Π-cells and by curve-fitting procedure in the case of CMT. In this case, excellent agreement has been obtained for all tested models, both in transmission and reflection, in a bandwidth of one octave. A further study plan is to include the effect of losses in the models and treat SRRs with arbitrarily positioned gaps.

Acknowledgments. This work has been supported by Serbian Ministry of Education, Science and Technological Development through grants TR-32024 and III-45016.

Author ORCIDs. Vojislav Milosevic, 0000-0001-8113-7954

References

1 **Smith DR, Padilla WJ, Vier DC, Nemat-Nasser SC and Schultz S** (2000) Composite medium with simultaneously negative permeability and permittivity. *Physical Review Letters* **84**, 4184–4187.

2 **Caloz C and Itoh T** (2005) *Electromagnetic Metamaterials: Transmission Line Theory and Microwave Applications*. Hoboken, New Jersey: Wiley.

3 **Alibakhshi-Kenari M, Naser-Moghadasi M, Ali Sadeghzadeh R, Singh Virdee B and Limiti E** (2016) New compact antenna based on simplified crlh-tl for uwb wireless communication systems. International Journal of RF and Microwave Computer-Aided Engineering **26**, 217–225.

4 **Martin F, Falcone F, Bonache J, Marques R and Sorolla M** (2003) Miniaturized coplanar waveguide stop band filters based on multiple tuned split ring resonators. *IEEE Microwave and Wireless Components Letters* **13**, 511–513.

5 **Naqui J, Durán-Sindreu M and Martín F** (2012) Alignment and position sensors based on split ring resonators. *Sensors* **12**, 11790–11797. [Online]. Available: http://www.mdpi.com/1424-8220/12/9/11790.

6 **Boskovic N, Jokanovic B and Radovanovic M** (2017) Printed frequency scanning antenna arrays with enhanced frequency sensitivity and sidelobe suppression. *IEEE Transactions on Antennas and Propagation* **65**, 1757–1764.

7 **Naqui J, Fernandez-Prieto A, Duran-Sindreu M, Mesa F, Martel J, Medina F and Martin F** (2012) Common-mode suppression in microstrip differential lines by means of complementary split ring resonators: Theory and applications. *IEEE Transactions on Microwave Theory and Techniques* **60**, 3023–3034.

8 **Alibakhshi-Kenari M, Naser-Moghadasi M and Sadeghzadeh RA** (2015) Bandwidth and radiation specifications enhancement of monopole antennas loaded with split ring resonators. *IET Microwaves, Antennas Propagation* **9**, 1487–1496.

9 **Milosevic V, Jokanovic B and Kolundzija B** (2010) Microwave stereometamaterials and parameter extraction. *4th International Congress on Advanced Electromagnetic Materials in Microwaves and Optics (METAMATERIALS)*.

10 **Naqui J, Duran-Sindreu M and Martin F** (2013) Modeling split-ring resonator (srr) and complementary split-ring resonator (csrr) loaded transmission lines exhibiting cross-polarization effects. *IEEE Antennas and Wireless Propagation Letters* **12**, 178–181.

11 **Baena JD, Bonache J, Martin F, Sillero RM, Falcone F, Lopetegi T, Laso MAG, Garcia-Garcia J, Gil I, Portillo MF and Sorolla M** (2005) Equivalent-circuit models for split-ring resonators and complementary split-ring resonators coupled to planar transmission lines. *IEEE Transactions on Microwave Theory and Techniques* **53**, 1451–1461.

12 **Aznar F, Bonache J and Martín F** (2008) Improved circuit model for left-handed lines loaded with split ring resonators. *Applied Physics Letters* **92**, 043512.

13 **Bojanic R, Milosevic V, Jokanovic B, Medina-Mena F and Mesa F** (2014) Enhanced modelling of split-ring resonators couplings in printed circuits. *IEEE Transactions on Microwave Theory and Techniques* **62**, 1605–1615.

14 **Tassin P, Zhang L, Koschny T, Economou EN and Soukoulis CM** (2009) Low-loss metamaterials based on classical electromagnetically induced transparency. *Physical Review Letters* **102**, 053901. [Online]. Available: https://link.aps.org/doi/10.1103/PhysRevLett.102.053901.

15 **Milosevic V, Jokanovic B, Bojanic R and Jelenkovic B** (2013) Classical electromagnetically induced transparency in metamaterials. *Microwave Review* **19**, 76–81.

16 **Kurter C, Tassin P, Zhang L, Koschny T, Zhuravel AP, Ustinov AV, Anlage SM and Soukoulis CM** (2011) Classical analogue of electromagnetically induced transparency with a metal-superconductor hybrid metamaterial. *Physical Review Letters* **107**, 043901. [Online]. Available: https://link.aps.org/doi/10.1103/PhysRevLett.107.043901.

17 **Haus HA and Huang W** (1991) Coupled-mode theory. *IEEE* Proceedings **79**, 1505–1518.

18 **Fan S, Suh W and Joannopoulos JD** (2003) Temporal coupled-mode theory for the fano resonance in optical resonators. *Journal of the Optical Society of America A* **20**, 569–572. [Online]. Available: http://josaa.osa.org/abstract.cfm?URI=josaa-20-3-569.

19 **Jovanovic S, Milovanovic B and Gmitrovic M** (2013) Theory and realization of simple bandpass filters with antiparallel configuration. *Progress In Electromagnetics Research* **136**, 101–122.

20 **Tassin P, Zhang L, Zhao R, Jain A, Koschny T and Soukoulis CM** (2012) Electromagnetically induced transparency and absorption in

https://doi.org/10.1017/S1759078719000308 Published online by Cambridge University Press

metamaterials: The radiating two-oscillator model and its experimental confirmation. *Physical Review Letters* **109**, 187401.
21 **Haus H** (1984) *Waves and Fields in Optoelectronics*, ser. Prentice-Hall Series in Solid State Physical Electronics. Englewood Cliffs, New Jersey: Prentice Hall, Incorporated.
22 **Lopetegi T, Laso MAG, Erro MJ, Sorolla M and Thumm M** (2002) Analysis and design of periodic structures for microstrip lines by using the coupled mode theory. *IEEE Microwave and Wireless Components Letters* **12**, 441–443.
23 **Fu Q, Zhang F, Fan Y, Dong J, Cai W, Zhu W, Chen S and Yang R** (2017) Weak coupling between bright and dark resonators with electrical tunability and analysis based on temporal coupled-mode theory. *Applied Physics Letters* **110**, 221905.
24 **Suh W, Wang Z and Fan S** (2004) Temporal coupled-mode theory and the presence of non-orthogonal modes in lossless multimode cavities. *IEEE Journal of Quantum Electronics* **40**, 1511–1518.
25 **Hong J and Lancaster M** (2004) *Microstrip Filters for RF / Microwave Applications*, ser. Wiley Series in Microwave and Optical Engineering. Hoboken, New Jersey: Wiley.
26 **Djordjevic A, Bazdar M, Sarkar T and Harrington R** (1999) *Linpar for Windows: Matrix Parameters for Multiconductor Transmission Lines, Software and User's Manual, Version 2.0*, ser. Artech House microwave library. Norwood, Massachusetts: Artech House.
27 **Lagarias JC, Reeds JA, Wright MH and Wright PE** (1998) Convergence properties of the Nelder–Mead simplex method in low dimensions. *SIAM Journal on Optimization* **9**, 112–147.

Vojislav Milosevic was born in Belgrade, Serbia, on April 5, 1986. He received the Dipl. Ing. and M.Sc. degrees in electrical engineering at the University of Belgrade, Faculty of Electrical Engineering, Belgrade, Serbia, in 2009 and 2012, respectively. He is currently pursuing a Ph.D. degree at the University of Belgrade. In 2010 he started working as a research assistant at the Photonic Center, Institute of Physics, Belgrade, Serbia, where he is involved with electromagnetic metamaterials and their applications.

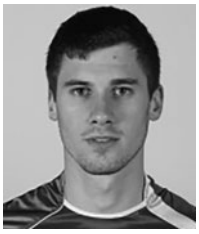

Radovan Bojanic was born in Knin, Croatia, in 1986. He received the Dipl.Ing. and M.Sc. degrees in electrical engineering at the University of Belgrade, Faculty of Electrical Engineering, Belgrade, Serbia, in 2009 and 2012, respectively. From 2010 to 2014 he worked at the Institute of Physics, Belgrade, Serbia as a research assistant in the Photonic Center, where he was involved in modelling and simulation of microwave circuits. Since 2015 he has been pursuing a PhD degree at Eindhoven University of Technology, Netherlands.

Branka Jokanovic (M'89) received the Dipl. Ing., M.Sc. and Ph.D. degrees in electrical engineering at the University of Belgrade, Faculty of Electrical Engineering, Belgrade, Serbia, in 1977, 1988, and 1999, respectively. She is currently a Research Professor at the Institute of Physics, University of Belgrade, Serbia. Before she joined the Photonic Center, Institute of Physics, she was the Head of the Microwave Department, Institute IMTEL, Belgrade. Her current research interests include modelling, simulation and characterization of microwave and photonic metamaterials for wireless communications and sensors.

https://doi.org/10.1017/S1759078719000308 Published online by Cambridge University Press